Effects of sample preparation on the microstructural signatures of faulting in clay-bearing fault gouge

K. Aiyama[a,*], K. Mizoguchi[a], K. Hirano[b], S. Takizawa[a,c]

[a] *Central Research Institute of Electric Power Industry, 1646 Abiko, Abiko, Chiba, 270-1194, Japan*
[b] *Ceres, Inc., 1646 Abiko, Abiko, Chiba, 270-1166, Japan*
[c] *National Research Institute for Earth Science and Disaster Resilience, 3-1 Tennodai, Tsukuba, Ibaraki, 305-0006, Japan*

ABSTRACT

Clay-rich fault gouge in the principal slip zones of faults stores abundant water within pores and between clay interlayers. During the preparation of thin-sections and rock chips for microstructural observations, fault-gouge samples are commonly air-dried at room temperature or in an oven. However, during the drying process, remnant liquid water between gouge grains produces an inter-particle adhesion force (liquid-bridge force), which rearranges the grain-to-grain structure, likely resulting in a disturbance of the original fabric. For this study, we prepared gouge samples from the Itozawa fault, northeastern Japan, using a *t*-butyl alcohol freeze-drying method that mitigates drying-induced fabric disturbance. We then compared the microstructure of our samples with those prepared using the conventional air-drying method. The freeze-dried samples preserve a smooth fault plane, clearly defined nanoparticles, and well-developed shear-sense indicators, including slickenlines and Riedel shear planes. In contrast, the air-dried samples underwent shrinkage during drying, which distorted the geometry of the fault plane. These air-dried samples lack nanoparticles and display only a weak shear fabric. We conclude that microstructural observations on samples prepared using the *t*-butyl alcohol freeze-drying method, compared with conventional air-drying, could preserve more evidence for the retrieval of fault information, including the kinematics, slip stability, and dynamic weakening mechanism of a fault.

1. Introduction

The principal slip zones of faults comprise fine-grained gouge that commonly contains abundant clay minerals (e.g., Otsuki et al., 2003; Bullock et al., 2014). Microstructural analysis of fault gouge using scanning electron microscopes (SEMs) can constrain the deformation processes associated with past slip events (Boullier et al., 2009). Until the 1970s, incohesive fault rocks were assumed to exhibit random fabrics (e.g., Sibson, 1977); however, more recent field and laboratory investigations have recognized Riedel shear planes in such rocks (e.g., Logan et al., 1979; Chester et al., 1985; Rutter et al., 1986; Tanaka, 1992a). Slickensides with slickenlines and Riedel shear planes preserved in fault rocks can be used to determine the sense of shearing during fault motion (e.g., Logan et al., 1979; Doblas, 1998). The degree of development of such structures in fault gouge is closely related to the stability of fault slip, which is associated with earthquake nucleation (Beeler et al., 1996). As well as fault kinematics, shear-sense indicators can be used to constrain paleostress tensors and tectonic activity around

faults (e.g., Petit, 1987; Chorowicz et al., 1999). SEM observations have revealed the micro-to nano-scale morphology and size distribution of gouge grains, which can be used to constrain weakening mechanisms during faulting (e.g., frictional melting, thermal pressurization, powder lubrication and graphization of gouge; Hirono et al., 2006; Han et al., 2007; Boullier et al., 2009; Han et al., 2010, 2014; Kuo et al., 2014b).

Prior to the preparation of thin-sections and rock chips for micro-structural observations, clay-rich gouge samples are typically air- or oven-dried to remove water in pores and adsorbed onto the surfaces of clay minerals, which have large water storage capacities owing to their high specific surface area. During these drying methods, the surface tension force associated with water in the samples can potentially disrupt or destroy original fabrics (e.g., Gillott, 1969; Bennett and Hulbert, 1986). Several sample preparation methods have been developed over the past few decades for soft sediments and soils containing abundant clay minerals (i.e., similar to fault gouge), including the freeze-drying method used for the preparation of SEM specimens (e.g., Gillott, 1969; Bennett and Hulbert, 1986; Takizawa et al., 1995; Takizawa, 1997).

This method preserves the grain-to-grain structural integrity of soft-sediment samples and has revealed a change in the fabric of submarine sediments with increasing burial depth, from randomly oriented particles with edge-to-face contacts to highly oriented and densely packed particles, corresponding to a decrease in void ratio (Bennett and Hulbert, 1986). However, few studies have examined how drying affects the fabric of fault-gouge samples used to determine fault kinematics (Takagi and Kobayashi, 1996; Oohashi et al., 2008).

In this contribution, we used a *t*-butyl alcohol freeze-drying method (Takizawa et al., 1995; Takizawa, 1997) to prepare samples of clay-rich fault gouge for microstructural analysis. The samples were collected from the Itozawa fault immediately after it ruptured during the Mw 6.6 Hamadoori earthquake in April 2011. We compare the microstructures of samples prepared using freeze-drying and conventional air-drying methods. We show that the drying process can result in the inaccurate identification of kinematic markers and produce erroneous conclusions on slip stability and weakening mechanisms during faulting. In section 2, we describe the theoretical background for drying-induced disturbance. In section 3, we describe the methods used for this study and give details of the X-ray diffraction (XRD) and SEM techniques used for microstructural analysis. The Itozawa fault is described in section 4, and the microstructural results and a discussion are provided in section 5. Section 6 presents the conclusions of the study.

2. Inter-particle forces associated with dehydration: theoretical background

Fault rocks comprise particles of various sizes, with several adhesion forces acting between the particles. The main adhesion forces are van der Waals, electrostatic, and liquid-bridge forces. A liquid bridge forms between two particles when liquid is present in the gap between those particles (Fig. 1, central part), producing a force that has been theoretically and experimentally analyzed (e.g., Iinoya and Muramoto, 1967; Endo and Kousaka, 1993). The magnitude of this force is proportional to the surface tension force of the liquid (e.g., Yamamoto and Matsuyama, 1991; Masuda et al., 2006). Israelachvili (1991) showed that the surface tension force of water (73 mN/m at 20 °C) is higher than that of many other liquids (e.g., acetone, ethanol, and benzene, which exhibit surface tension forces at 20 °C of 23.7, 22.8 and 28.8 mN/m, respectively). Thus, the liquid-bridge force associated with water is stronger than that of other liquids. For particles with diameters of < 1 mm, the liquid-bridge force is stronger than the van der Waals and electrostatic forces. Furthermore, the dominance of the liquid-bridge force is negatively correlated with particle diameter (e.g., Yamamoto and Matsuyama, 1991; Masuda et al., 2006). Thus, clay particles, defined as having diameters of < 2 μm, are significantly affected by the liquid-bridge force associated with water.

Water vaporization during air- or oven-drying results in the formation of liquid bridges, generating liquid-bridge forces that act on submillimeter particles, causing them to aggregate (Fig. 1). De Souza (2007) and Payam and Fathipour (2011) found that the more hydrophilic the surfaces of particles connected by a liquid bridge, the greater the magnitude of the liquid-bridge force. Among clay minerals frequently observed in fault gouge, smectite crystal surfaces are the most hydrophilic (Kawamura, 2008). Therefore, when wet samples containing smectite are air- or oven-dried, smectite crystal aggregation is enhanced, which changes the distribution of smectite crystals and the overall rock fabric.

3. Methods

We collected four gouge samples from the principal slip zone of the Itozawa fault (samples A to D). The mineralogy of the gouge samples is
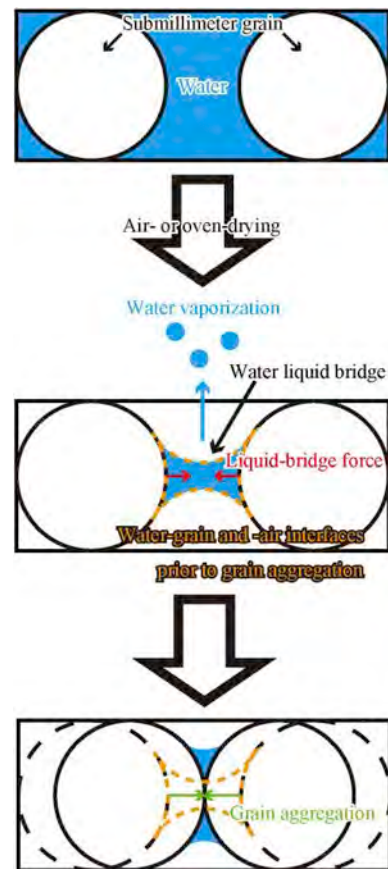

Fig. 1. Schematic diagram illustrating the mechanism of grain aggregation in response to air- or oven-drying.

described in section 4. Samples A and B were prepared using the air-drying method. These two samples were completely dehydrated by allowing natural drying to occur for approximately one year, starting immediately after sampling.

Samples C and D were prepared using the freeze-drying technique. As samples containing abundant water begin to dehydrate when exposed to air, these samples were immediately packed into polypropylene bags filled with ethanol and bound with cotton yarn to prevent sample collapse during transport to the laboratory (Fig. 2). Pure

Fig. 2. Photograph of a bagged gouge sample in the field.

Fig. 3. Photograph of a sample undergoing ethanol substitution in preparation for the *t*-butyl alcohol freeze-drying method.

ethanol is highly miscible with water and is commonly used as a dehydrating agent (e.g., Tanaka, 1992b). Therefore, we used a 70% ethanol solution to prevent the aggregation of grains due to the rapid dehydration of water.

Samples C and D were dehydrated by replacing water in the samples with ethanol, before employing the *t*-butyl alcohol freeze-drying method. Ethanol substitution is commonly used during the pre-treatment of samples; however, as ethanol is highly volatile, care must be taken to prevent air-drying of samples during the ethanol substitution process. The *t*-butyl alcohol freeze-drying method was performed as follows: (1) Ethanol in the samples was replaced with *t*-butyl alcohol; (2) the samples were frozen, and the *t*-butyl alcohol was sublimated. *t*-Butyl alcohol is miscible with ethanol (Tanaka, 1992b) and exhibits a high freezing point (25.5 °C; Tanaka, 1992b) and a high vapor pressure (40.7 mm Hg at 25 °C; U.S. National Library of Medicine, 2014), allowing it to be quickly and easily frozen and sublimated.

The ethanol substitution and *t*-butyl alcohol freeze-drying methods are described in detail in sections 3.1 and 3.2, respectively, and the effects of the air-drying and *t*-butyl alcohol freeze-drying methods on pure smectite samples are presented in section 3.3. We examined the microstructures of samples A to D using an SEM. SEM observations on samples A and C were conducted on specimens cut along the XZ plane (i.e., parallel to slickenlines and perpendicular to the fault plane). For samples B and D, SEM observations were performed on specimens oriented normal to the fault plane. Microstructural observations were conducted using a JSM-7001F SEM at the Central Research Institute of Electric Power Industry (CRIEPI), Chiba, Japan. The mineralogy of the samples was determined using an X'Pert MRD Pro PW3040 XRD with CuKα radiation at the CRIEPI. XRD measurements were conducted from 2° to 70° 2θ with a 2°/min scan speed, a 45 kV accelerating voltage, and a 40 mA current. The XRD was equipped with auto divergence and anti-scatter slits as well as a 0.2 mm receiving slit.

3.1. Ethanol substitution

Water in samples C and D was replaced with ethanol as follows: (1) The samples were immersed in ethanol for 7 days; (2) a mixture of water and ethanol was removed from the samples and replaced with ethanol; (3) steps (1) and (2) were repeated four times. To prevent rapid dehydration, the samples were immersed in a 70% ethanol solution for the first iteration of steps (1) and (2), followed by 100% ethanol thereafter. Approximately one month was required to complete ethanol substitution in the samples. Owing to the tight packaging of the samples, some parts were not in direct contact with ethanol. Therefore, we wrapped the samples with paper towels to ensure that the entire surface of the sample was in contact with ethanol (Fig. 3).

3.2. t-Butyl alcohol freeze-drying method for SEM observations

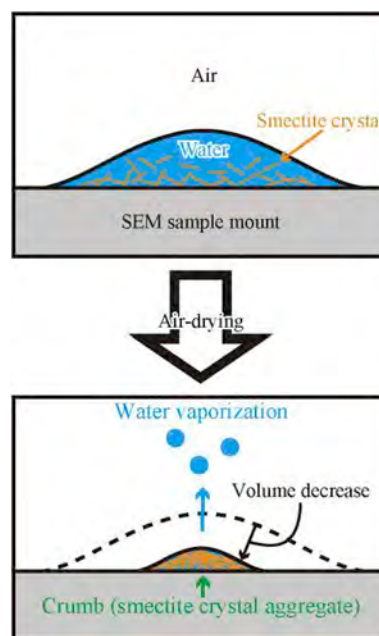This procedure was conducted used *t*-butyl alcohol, liquid nitrogen, and a freeze dryer.

Fig. 5. Schematic diagram illustrating the mechanism of smectite crystal aggregation in response to air-drying.
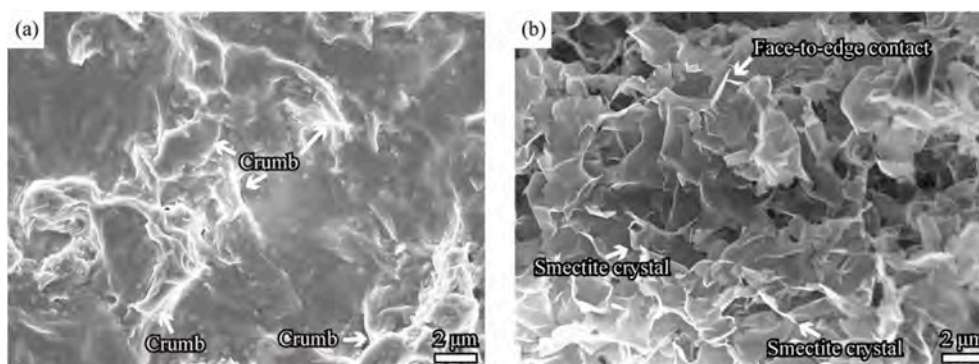

Fig. 4. SEM photomicrographs of (a) air-dried and (b) *t*-butyl alcohol freeze-dried pure smectite samples collected from the Tsukinuno bentonite mine in Yamagata Prefecture, Japan.
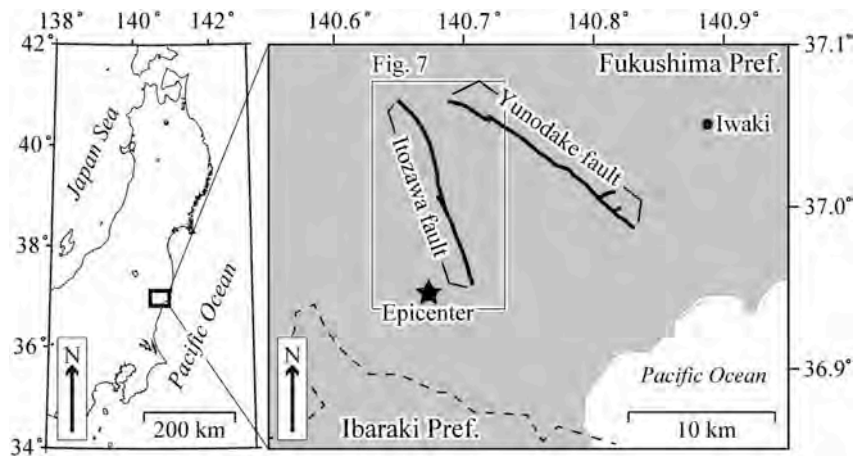
Fig. 6. Simplified map of the Itozawa and Yunodake faults that slipped during the 2011 Hamadoori earthquake. The solid star indicates the epicenter of the earthquake.

3.2.1. t-Butyl alcohol substitution

Ethanol in dehydrated samples C and D was replaced by *t*-butyl alcohol as follows: (1) The samples were immersed in *t*-butyl alcohol for one week; (2) a mixture of ethanol and *t*-butyl alcohol was removed from the samples and replaced with *t*-butyl alcohol; (3) steps (1) and (2) were repeated five times. During *t*-butyl alcohol substitution, the samples were kept above the freezing point of *t*-butyl alcohol (25.5 °C).

3.2.2. Freeze-drying

Following *t*-butyl alcohol substitution, samples C and D were frozen and the *t*-butyl alcohol was then sublimated as follows: (1) The samples were frozen rapidly using liquid nitrogen; (2) the frozen *t*-butyl alcohol was sublimated under vacuum using a HITACHI ES-2030 freeze dryer. The samples were kept below 25.5 °C during freeze-drying to avoid melting of *t*-butyl alcohol. Freezing was conducted rapidly to prevent the formation of large crystals that may damage faulting-related microstructures.
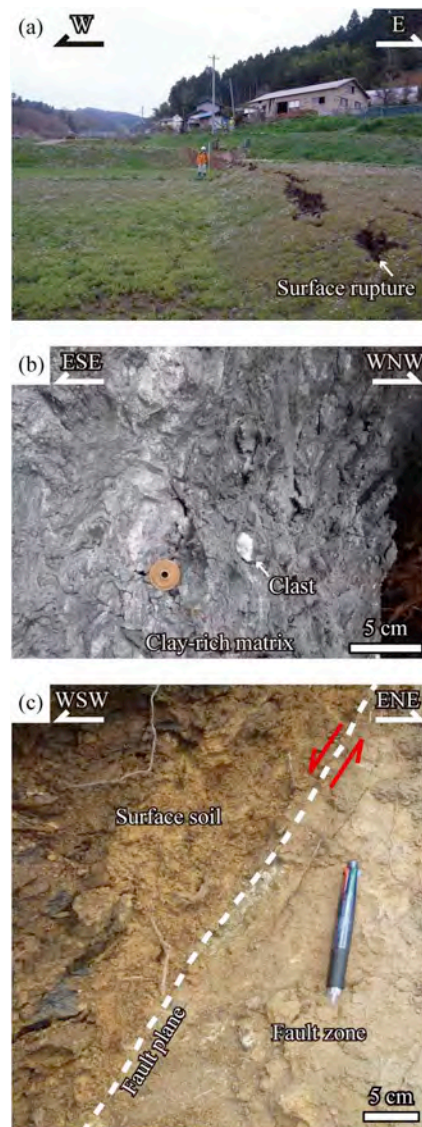

Fig. 7. Simplified geological map of the Itozawa fault.

Fig. 8. Photographs of a surface rupture (a) and the fault zone (b and c) of the Itozawa fault. Red arrows indicate the slip direction. Locations of the photographs are shown in Fig. 7. . (For interpretation of the references to colour in this figure legend, the reader is referred to the Web version of this article.)

3.3. Effects of the air-drying and t-butyl alcohol freeze-drying methods on pure smectite samples

Edge-to-face contacts between clay crystals form in unconsolidated sediments deposited in pure water (e.g., Bennett and Hulbert, 1986). However, this contact structure is extremely fragile and can be destroyed by air- and oven-drying. Smectite-bearing fault rocks occur in many faults (e.g., Otsuki et al., 2003; Kuo et al., 2009; Noda and Shimamoto, 2009; Casciello et al., 2011; Holdsworth et al., 2011; Haines and van der Pluijm, 2012). To determine the effect of air-drying and *t*-butyl alcohol freeze-drying methods on smectite-bearing samples, we compare our samples with those collected from the Tsukinuno bentonite mine in Yamagata Prefecture, Japan. For SEM observations, smectite samples were mixed with pure water to allow edge-to-face contacts to be observed. The air-dried sample of Tsukinuno bentonite was prepared by placing mixed smectite crystals on an SEM sample mount and then air-drying for one day. This sample does not display clearly defined smectite crystals and includes several "crumbs" (i.e., smectite crystal aggregates) with various shapes and sizes (Fig. 4a). In contrast, individual euhedral smectite crystals were recognized in the *t*-butyl alcohol freeze-dried sample of Tsukinuno bentonite (Fig. 4b), and lamellar smectite crystals exhibit edge-to-face contacts. Thus, we conclude that the *t*-butyl alcohol freeze-drying method can suppress the aggregation of fine-grained clay minerals during dehydration. Smectite crystals in the air-dried sample were subjected to strong liquid-bridge forces during dehydration, resulting in the aggregation of crystals (Fig. 5), which prevented the identification of individual smectite crystals.

4. Itozawa fault

The April 2011 Hamadoori earthquake (Mw 6.6) occurred in Fukushima Prefecture, northeastern Japan (Fig. 6). The NNW-striking Itozawa and NW-striking Yunodake faults ruptured during the earthquake, and a maximum westward/normal-slip displacement of about 2 m occurred along the Itozawa fault (Mizoguchi et al., 2012). Borehole and trench surveys following the earthquake revealed that the Itozawa

fault has ruptured at least three times during the last 50,000 years (Kurosawa et al., 2012; Tsutsumi and Toda, 2012; Niwa et al., 2013; Toda and Tsutsumi, 2013). The Itozawa fault transects Early Cretaceous schist, which is widespread in the Hamadoori area (Kubo et al., 2007) (Fig. 7).

The earthquake surface rupture (Site 1 in Fig. 7; Fig. 8a) was identified during a field survey conducted immediately after the 2011 earthquake. The Itozawa fault zone was also observed at two sites located to the SSE of Site 1 (Sites 2 and 3 in Fig. 7). Gouge from the fault zone is clay-rich and contains abundant water (Fig. 8b). Maximum displacement at Site 3 occurred along a fault plane that strikes N27°W, dips 75°W, and separates loose surface soil from a 4-cm-thick gouge zone derived from Early Cretaceous schist (Mizoguchi et al., 2012, Fig. 8c). Slickenlines on the fault plane trend N60°E and plunge 68°SW. Samples A to D were collected from the principal slip zone along the fault plane immediately following the 2011 earthquake. XRD analysis indicates that the sampled gouge comprises smectite, quartz, and plagioclase (Fig. 9).

5. Results and discussion

SEM photomicrographs on the XZ plane of sample A (prepared using the air-drying method) reveal a substantially distorted fault plane (Fig. 10a) and a lack of clear Riedel shear planes close to the fault plane (Fig. 10b and c). In contrast, sample C (prepared using the *t*-butyl alcohol freeze-drying method) displays a smooth fault plane (at 100 × magnification; Fig. 10d) that contains step structures due to the presence of Riedel shear planes (Fig. 10e and f).

As our samples were collected from the fault plane that slipped during the 2011 earthquake, we expected them to preserve Riedel shear planes indicating normal slip. However, in contrast to sample C, sample A does not contain Riedel shear planes. Smectite crystals in sample A were likely aggregated during air-drying, similar to the air-dried smectite sample collected from the Tsukinuno bentonite mine. We therefore conclude that any Riedel shear planes that were present in sample A were destroyed during smectite crystal aggregation and an associated change in the distribution and morphology of smectite
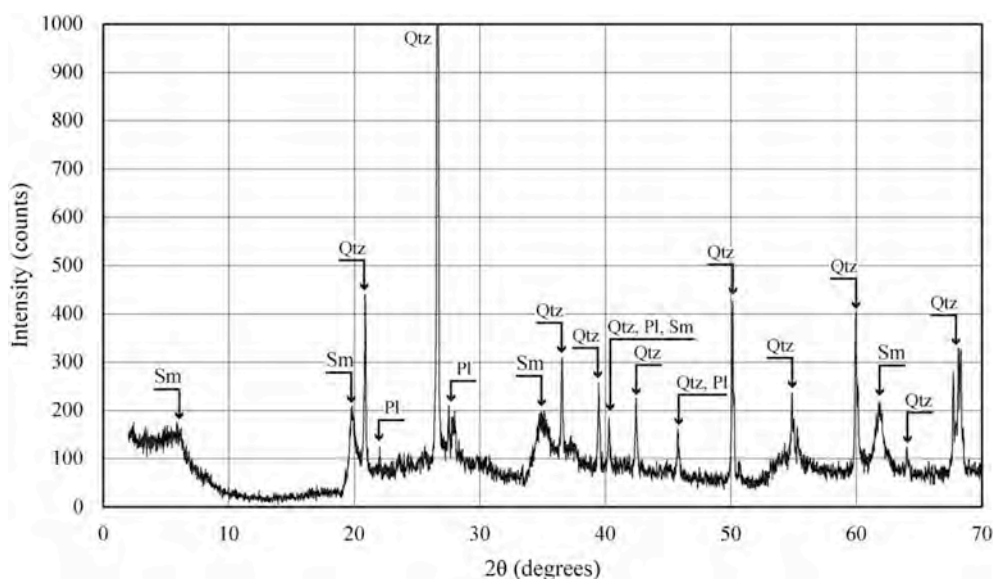

Fig. 9. Whole-rock XRD pattern for a fault-gouge sample from the Itozawa fault. Qtz = quartz; Pl = plagioclase; Sm = smectite. The fault gouge was sampled from the outcrop shown in Fig. 8c (Site 3 in Fig. 7).
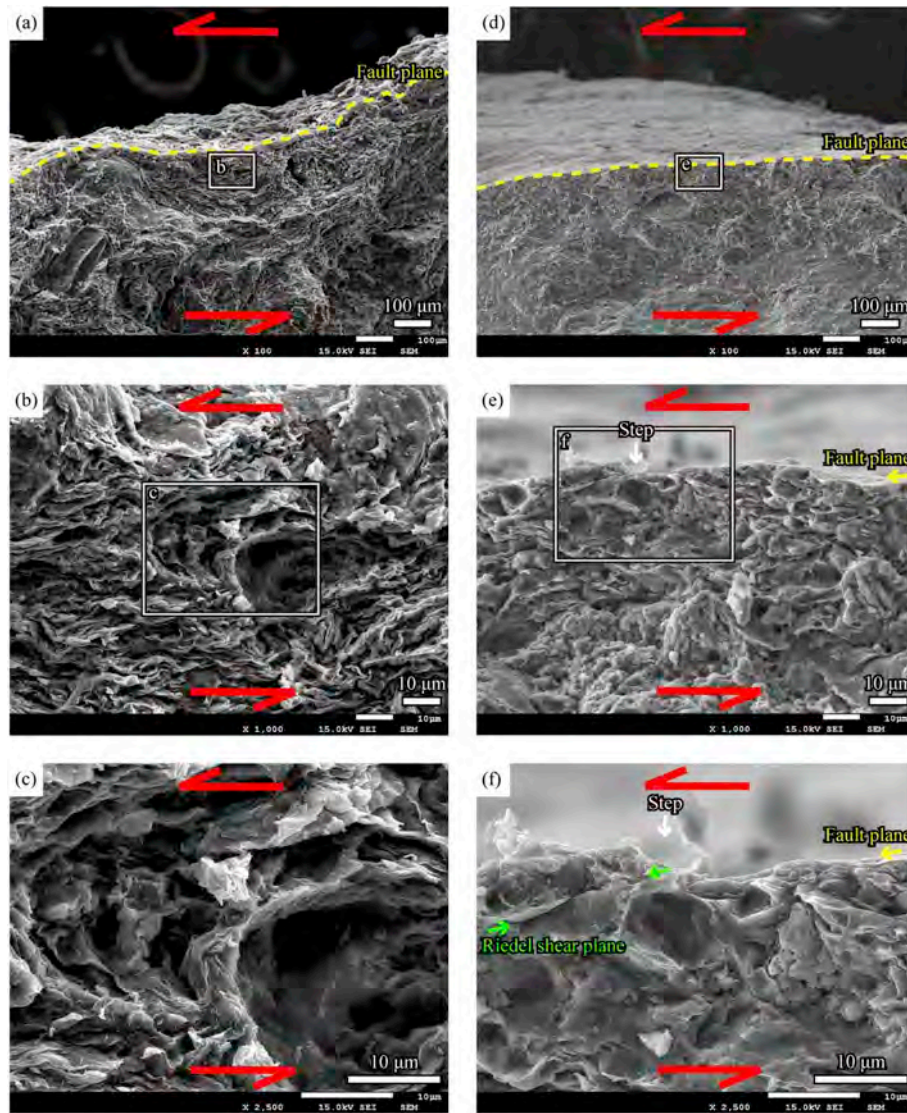
Fig. 10. SEM photomicrographs of the XZ plane of (a–c) sample A and (d–f) sample C. Samples A and C were prepared using air-drying and *t*-butyl freeze-drying methods, respectively. Red arrows indicate the slip direction. . (For interpretation of the references to colour in this figure legend, the reader is referred to the Web version of this article.)

crystals.

Gouge from the Itozawa fault comprises three distinct minerals: smectite, quartz, and plagioclase (Fig. 9). As the liquid-bridge force is dependent on mineralogy (Kawamura, 2008), the degree of particle aggregation (and volume reduction) will vary across the samples. Therefore, we infer that the fault plane in sample A, which was likely smooth prior to air-drying, was distorted as a result of non-uniform shrinkage during air-drying. Furthermore, a non-uniform distribution of pore water (e.g., due to heterogeneous particle size) will also induce non-uniform shrinkage during air-drying, resulting in the distortion of sample surfaces (Fig. 11). However, monomineralic samples with homogeneous particle size and pore water distribution may not undergo surface distortion during air-drying. A large ($\sim$200 μm) quartz/plagioclase grain is observed beneath a convex segment of the distorted fault plane in sample A (lower-left corner of Fig. 10a).

SEM photomicrographs of sample B (prepared using the air-drying method) taken normal to the fault plane reveal weak slickenlines on a rough fault plane (Fig. 12a; 200 $\times$ magnification). The fault plane comprises a variety of "crumbs" with various shapes and sizes (Fig. 12b). The surfaces of these crumbs are characterized by nanoscale "nubs" (Fig. 12c). No nanoparticles were observed on the fault-plane surface or along the edges of voids.

In contrast, SEM images of sample D (prepared using the *t*-butyl alcohol freeze-drying method) display abundant slickenlines on a smooth fault plane at 200 $\times$ and 2500 $\times$ magnifications (Fig. 12d and e). Nanoparticles (diameter = 100–200 nm) occur on the fault plane (Fig. 12f) and along the edges of voids on the fault plane.

Slickenlines are formed when particles sandwiched between fault surfaces erode the surfaces during fault slip (Doblas, 1998). Therefore, the presence of slickenlines indicates that the surfaces have undergone brittle slip in the shallow crust (i.e., faulting, such as the 2011 Hamadoori and the 1999 Chi-Chi earthquakes; Hashimoto et al., 2015). Thus,
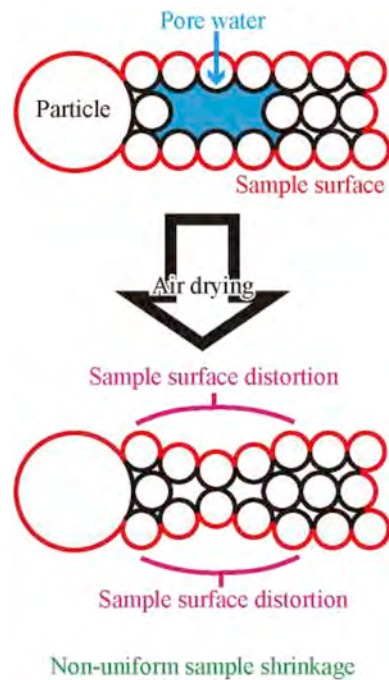
Fig. 11. Schematic diagram illustrating the mechanism of sample surface distortion in response to non-uniform sample shrinkage.

the fault plane of sample D records faulting in the shallow crust, whereas that of sample B does not. Moreover, sample D contains nanoparticles on a smooth fault plane. A similar, smectite-rich sample from the Tsukinuno bentonite (prepared using the *t*-butyl alcohol freeze-drying method) does not contain nanoparticles. If the nanoparticles in sample D formed as a result of chemical contamination during the *t*-butyl alcohol freeze-drying method, nanoparticles would also have formed in the sample from the Tsukinuno bentonite mine. Therefore, we conclude that nanoparticles in sample D were derived from smectite crystals and were not formed via chemical contamination.

Previous laboratory and field studies have attributed the formation of nanoparticles in clay-bearing faults to the (1) thermal decomposition and (2) hydrothermal alteration of clay minerals, and (3) grain comminution (e.g., Ujiie et al., 2011; Hirono et al., 2014; Smeraglia et al., 2017a). Han et al. (2010) identified nanoparticles on a fault plane produced in a laboratory friction experiment performed at seismic slip rates and suggested that fault weakening occurs in response to powder lubrication due to nanoparticle rolling. Although the formation mechanism of nanoparticles in sample D was not investigated in the present study, the presence of nanoparticles would have facilitated slip propagation during the April 2011 Hamadoori earthquake rupture.

Sample B displays only weak slickenlines and a rough fault plane. The weak slickenlines do not definitively indicate that the fault plane underwent brittle slip. No nanoparticles were observed in sample B, and the fault plane comprises several crumbs of various shapes and sizes. Chen et al. (2011) showed that the magnitude of the liquid-bridge force between two particles of different size increases with decreasing size difference. The nanoparticles in sample D display a relatively uniform size (diameter = 100–200 nm; Fig. 12f) and would therefore have been highly susceptible to the liquid-bridge force during air-drying. Furthermore, if the nanoparticles were small, highly aggregable smectite crystals (e.g., formed by grain comminution), the liquid-bridge force

between them during air-drying would have been especially strong.

As shown in section 3.3, particle aggregation during air-drying can restrict the identification of particles. Moreover, surfaces in sample D host nanoscale nubs. Therefore, the lack of individual nanoparticles in sample B may indicate that pre-existing nanoparticles were aggregated during air-drying to form the variably sized and shaped crumbs on the fault plane; nubs on these crumbs might represent original nanoparticles.

During laboratory friction experiments at sub-seismic slip rates, grains on rough slip surfaces aggregate during slip (Han et al., 2011; Aretusini et al., 2017). As the rough fault plane in sample B comprises grain aggregates, it may be misidentified as having formed at sub-seismic slip rates. Therefore, the air-drying of fault-rock samples, which affects the morphology of fault planes and causes aggregation of nanoparticles, can obscure fault-weakening mechanisms and lead to the misidentification of sub-seismic faults, which may, in reality, be seismic. Previous laboratory friction experiments have investigated the causal relationship between the formation of smooth slip planes and seismic/aseismic slip rates (e.g., Han et al., 2010, 2011; Oohashi et al., 2011; Tisato et al., 2012; Chen et al., 2013; Fondriest et al., 2013; Sagy et al., 2017; Orellana et al., 2018). However, our results indicate that the method of sample preparation can affect the smoothness of slip planes. Therefore, sample preparation methods should be carefully considered to allow accurate observations to be made of fault-plane morphology.

Nanoparticles have been observed in faults within carbonate rocks (e.g., Siman-Tov et al., 2013; Smeraglia et al., 2017a, 2017b); however, few have been reported from smectite-rich faults (Kuo et al., 2014a). If nanoparticles in smectite-rich faults are small smectite crystals, aggregation of such particles may have restricted their identification. Therefore, the application of the *t*-butyl alcohol freeze-drying sample preparation method may lead to the identification of nanoparticles in smectite-rich faults, and thus allow the fault-weakening mechanisms of such faults to be constrained.

6. Summary and conclusions

We used SEM examinations of clay- and water-rich fault-gouge samples from the Itozawa fault in northeastern Japan to compare the effects of two different sample dehydration methods (air-drying and *t*-butyl alcohol freeze-drying) on microfabrics. We are able to draw the following conclusions.

(1) Air-dried gouge samples preserve distorted and rough fault planes with only weak slickenlines and no clear shear-sense indicators or nanoparticles. We conclude that the microstructural signatures of faulting were disturbed as a result of particle aggregation during air-drying.
(2) In contrast to the air-dried samples, samples prepared using the *t*-butyl alcohol freeze-drying method preserved microstructural faulting signatures, such as a smooth fault plane hosting nanoparticles, slickenlines, and Riedel shear planes.

Our results indicate that air-drying can greatly affect the microstructure of unconsolidated fault rocks. In contrast, water-saturated and clay-rich fault-gouge samples prepared using the *t*-butyl alcohol freeze-drying method can preserve microstructural faulting signatures. Investigations of such samples should improve our understanding of kinematics, slip stability, and weakening mechanisms during faulting.
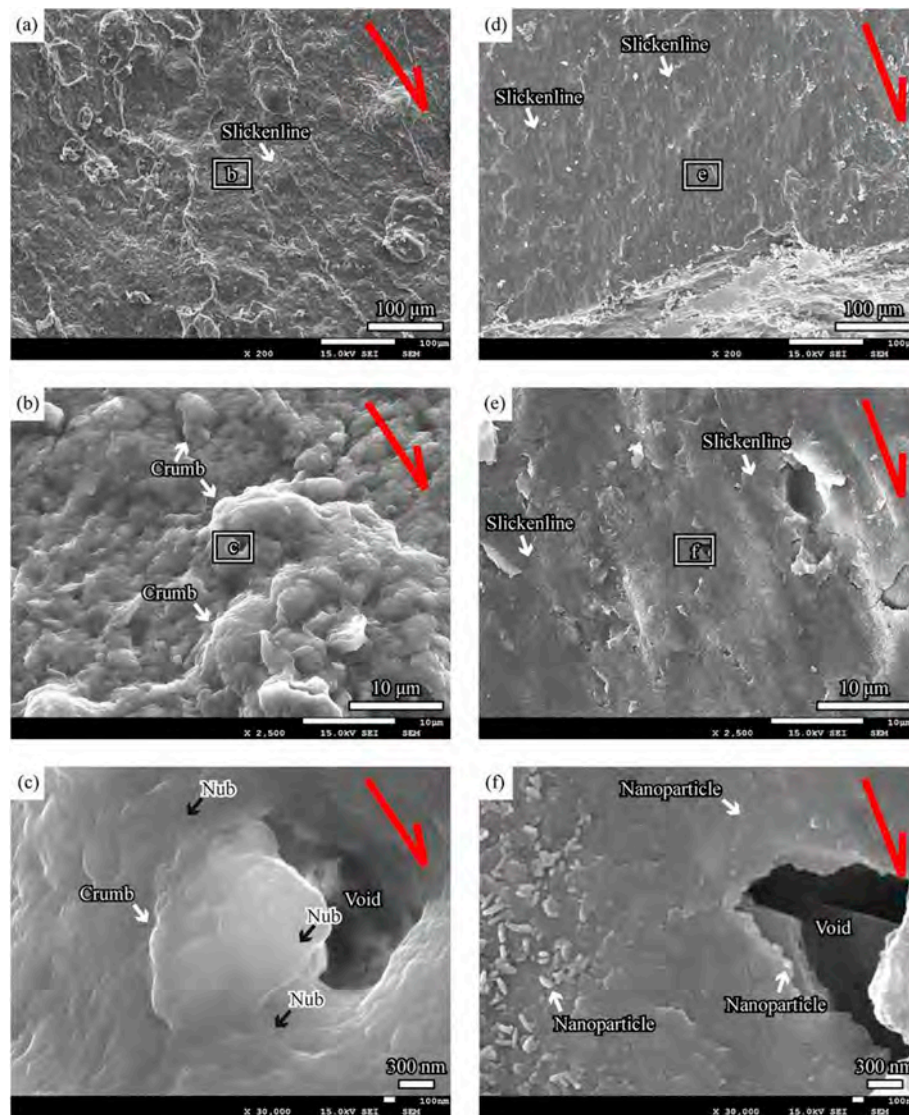
Fig. 12. SEM photomicrographs taken normal to the fault plane of (a–c) sample B and (d–f) sample D. Samples B and D were prepared using air-drying and *t*-butyl freeze-drying methods, respectively. Red arrows indicate the sense of motion of material above the fault plane. (For interpretation of the references to colour in this figure legend, the reader is referred to the Web version of this article.)

References

Aretusini, S., Mittempergher, S., Plümper, O., Spagnuolo, E., Gualtieri, A.F., Di Toro, G., 2017. Production of nanoparticles during experimental deformation of smectite and implications for seismic slip. Earth Planet. Sci. Lett. 488, 221–231. https://doi.org/10.1016/j.epsl.2017.01.048.

Beeler, N.M., Tullis, T.E., Blanpied, M.L., Weeks, J.D., 1996. Frictional behavior of large displacement experimental faults. J. Geophys. Res. 101 (No. B4), 8697–8715. https://doi.org/10.1029/96JB00411.

Bennett, R.H., Hulbert, M.H., 1986. Clay Microstructure. International Human Resources Development Corporation Press, Prentice Hall, Boston, MA.

Boullier, A.-M., Yeh, E.-C., Boutareaud, S., Song, S.-R., Tsai, C.-H., 2009. Microscale anatomy of the 1999 Chi-Chi earthquake fault zone. Geochem. Geophys. Geosyst. 10, Q03016. https://doi.org/10.1029/2008GC002252.

Bullock, R.J., Paola, N.D., Holdsworth, R.E., Trabucho-Alexandre, J., 2014. Lithological controls on the deformation mechanisms operating within carbonate-hosted faults during the seismic cycle. J. Struct. Geol. 58, 22–42. https://doi.org/10.1016/j.jsg.2013.10.008.

Casciello, E., Cosgrove, J.W., Cesarano, M., Romero, E., Queralt, I., Vergés, J., 2011.

Illite–smectite patterns in sheared Pleistocene mudstones of the Southern Apennines and their implications regarding the process of illitization: a multiscale analysis. J. Struct. Geol. 33, 1699–1711. https://doi.org/10.1016/j.jsg.2011.08.002.

Chen, X., Madden, A.S., Bickmore, B.R., Reches, Z., 2013. Dynamic weakening by nanoscale smoothing during high-velocity fault slip. Geology 41, 739–742. https://doi.org/10.1130/G34169.1.

Chen, Y., Zhao, Y., Gao, H., Zheng, J., 2011. Liquid bridge force between two unequal-sized spheres or a sphere and a plane. Particuology 9, 378–380. https://doi.org/10.1016/j.partic.2010.11.006.

Chester, F.M., Friedman, M., Logan, J.M., 1985. Foliated cataclasites. Tectonophysics 111, 139–146. https://doi.org/10.1016/0040-1951(85)90071-X.

Chorowicz, J., Dhont, D., Gündoğdu, N., 1999. Neotectonics in the eastern North Anatolian fault region (Turkey) advocates crustal extension: mapping from SAR ERS imagery and Digital Elevation Model. J. Struct. Geol. 21, 511–532. https://doi.org/10.1016/S0191-8141(99)00022-X.

De Souza, E.J., 2007. The Effect of Capillary Forces on Adhesion of Biological and Artificial Attachment Devices. Doctoral dissertation. Universität Stuttgarthttps://doi.org/10.18419/opus-878.

Doblas, M., 1998. Slickenside kinematic indicators. Tectonophysics 295, 187–197. https://doi.org/10.1016/S0040-1951(98)00120-6.

Endo, Y., Kousaka, Y., 1993. Analysis of separation between two particles adhering by a liquid bridge. Kagaku Kogaku Ronbunshu 19, 1136–1142. https://doi.org/10.1252/kakoronbunshu.19.1136. (in Japanese with English abstract).

Fondriest, M., Smith, S.A.F., Candela, T., Nielsen, S.B., Mair, K., Di Toro, G., 2013. Mirror-like faults and power dissipation during earthquakes. Geology 41, 1175–1178. https://doi.org/10.1130/G34641.1.

Gillott, J.E., 1969. Study of fabric of fine-grained sediments with the scanning electron

microscope. J. Sediment. Petrol. 39, 90–105. https://doi.org/10.1306/74D71BEA-2B21-11D7-8648000102C1865D.

Haines, S.H., van der Pluijm, B.A., 2012. Patterns of mineral transformations in clay gouge, with examples from low-angle normal fault rocks in the western USA. J. Struct. Geol. 43, 2–32. https://doi.org/10.1016/j.jsg.2012.05.004.

Han, R., Shimamoto, T., Hirose, T., Ree, J.-H., Ando, J., 2007. Ultralow friction of carbonate faults caused by thermal decomposition. Science 316, 878–881. https://doi.org/10.1126/science.1139763.

Han, R., Hirose, T., Shimamoto, T., 2010. Strong velocity weakening and powder lubrication of simulated carbonate faults at seismic slip rates. J. Geophys. Res. 115, B03412. https://doi.org/10.1029/2008JB006136.

Han, R., Hirose, T., Shimamoto, T., Lee, Y., Ando, J., 2011. Granular nanoparticles lubricate faults during seismic slip. Geology 39, 599–602. https://doi.org/10.1130/G31842.1.

Han, R., Hirose, T., Jeong, G.Y., Ando, J., Mukoyoshi, H., 2014. Frictional melting of clayey gouge during seismic fault slip: experimental observation and implications. Geophys. Res. Lett. 41, 5457–5466. https://doi.org/10.1002/2014GL061246.

Hashimoto, Y., Tobe, K., Yeh, E.-C., Lin, W., Song, S.-R., 2015. Changes in paleostress and its magnitude related to seismic cycles in the Chelung-pu Fault, Taiwan. Tectonics 34, 2418–2428. https://doi.org/10.1002/2015TC004005.

Hirono, T., Ikehara, M., Otsuki, K., Mishima, T., Sakaguchi, M., Soh, W., Omori, M., Lin, W., Yeh, E.-C., Tanikawa, W., Wang, C.-Y., 2006. Evidence of frictional melting from disk-shaped black material, discovered within the Taiwan Chelungpu fault system. Geophys. Res. Lett. 33, L19311. https://doi.org/10.1029/2006GL027329.

Hirono, T., Kameda, J., Kanda, H., Tanikawa, W., Ishikawa, T., 2014. Mineral assemblage anomalies in the slip zone of the 1999 Taiwan Chi-Chi earthquake: ultrafine particles preserved only in the latest slip zone. Geophys. Res. Lett. 41, 3052–3059. https://doi.org/10.1002/2014GL059805.

Holdsworth, R.E., van Diggelen, E.W.E., Spiers, C.J., de Bresser, J.H.P., Walker, R.J., Bowen, L., 2011. Fault rocks from the SAFOD core samples: implications for weakening at shallow depths along the San Andreas Fault, California. J. Struct. Geol. 33, 132–144. https://doi.org/10.1016/j.jsg.2010.11.010.

Iinoya, K., Muramoto, H., 1967. Approximate calculation of adhesion force of a particle by liquid pendular ring. J. Soc. Mater. Sci. Jpn. 16, 352–357. https://doi.org/10.2472/jsms.16.352. (in Japanese with English abstract).

Israelachvili, J.N., 1991. Intermolecular and Surface Forces, second ed. Academic Press, New York.

Kawamura, K., 2008. Molecular simulations of mineral–water systems. Geochemistry 42, 115–132. https://doi.org/10.14934/chikyukagaku.42.115. (in Japanese with English abstract).

Kubo, K., Yanagisawa, Y., Yamamoto, T., Nakae, S., Takahashi, Y., Toshimitsu, S., Banno, Y., Miyachi, Y., Takahashi, M., Komazawa, M., Ohno, T., 2007. Geological Map of Japan 1:200,000, Shirakawa. Geological Survey of Japan, AIST (in Japanese with English abstract).

Kuo, L.-W., Song, S.-R., Yeh, E.-C., Chen, H.-F., 2009. Clay mineral anomalies in the fault zone of the Chelungpu Fault, Taiwan, and their implications. Geophys. Res. Lett. 36, L18306. https://doi.org/10.1029/2009GL039269.

Kuo, L.-W., Hsiao, H.-C., Song, S.-R., Sheu, H.-S., Suppe, J., 2014a. Coseismic thickness of principal slip zone from the Taiwan Chelungpu fault Drilling Project-A (TCDP-A) and correlated fracture energy. Tectonophysics 619–620, 29–35. https://doi.org/10.1016/j.tecto.2013.07.006.

Kuo, L.-W., Li, H., Smith, S.A.F., Di Toro, G., Suppe, J., Song, S.-R., Nielsen, S., Sheu, H.-S., Si, J., 2014b. Gouge graphitization and dynamic fault weakening during the 2008 Mw 7.9 Wenchuan earthquake. Geology 41, 23–30. https://doi.org/10.1130/G34862.1.

Kurosawa, H., Kagohara, K., Miwa, A., Sato, F., Imaizumi, T., Miyauchi, T., Hashimoto, S., Nakajima, H., Shirosawa, M., Uchida, J., 2012. The surface rupture associated with the April 2011 Fukushima-ken Hamadōri earthquake in northeast Japan: preliminary report of fault outcrop observation and borehole survey at Shionohira, Tabito Town, Iwaki City. Active Fault Res. 36, 23–30. https://doi.org/10.11462/afr.2012.36_23. (in Japanese with English abstract).

Logan, J.M., Friedman, M., Higgs, N., Dengo, C., Shimamoto, T., 1979. Experimental studies of simulated gouge and their application to studies of natural fault zones. USGS open file report In: Proceedings of Conference VIII. Analysis of actual fault zones in bedrock. 79–1239. pp. 305–343.

Masuda, H., Higashitani, K., Yoshida, H., 2006. Powder Technology Handbook, third ed. CRC Press, Boca Raton, Florida.

Mizoguchi, K., Uehara, S., Ueta, K., 2012. Surface fault ruptures and slip distributions of the Mw 6.6 11 April 2011 Hamadoori, Fukushima prefecture, northeast Japan, earthquake. Bull. Seismol. Soc. Am. 102, 1949–1956. https://doi.org/10.1785/0120110308.

Niwa, Y., Toda, S., Omata, M., Mori, Y., 2013. Paleoseismic events of the Itozawa fault prior to the 2011 fukushima-ken-hamadori earthquake revealed from a borehole survey at Shionohira, Iwaki City, Fukushima prefecture, Japan. Active Fault Res. 39, 1–8. https://doi.org/10.11462/afr.2013.39_1. (in Japanese with English abstract).

Noda, H., Shimamoto, T., 2009. Constitutive properties of clayey fault gouge from the Hanaore fault zone, southwest Japan. J. Geophys. Res. 114, B04409. https://doi.org/10.1029/2008JB005683.

Oohashi, K., Kobayashi, K., Mashima, H., 2008. A method for making thin sections and polished slubs of non-cohesive fault rocks containing swelling clay minerals. J. Geol. Soc. Jpn. 114, 423–431. https://doi.org/10.5575/geosoc.114.426. (in Japanese with English abstract).

Oohashi, K., Hirose, T., Shimamoto, T., 2011. Shear-induced graphitization of carbonaceous materials during seismic fault motion: experiments and possible implications for fault mechanics. J. Struct. Geol. 33, 1122–1134. https://doi.org/10.1016/j.jsg.2011.01.007.

Orellana, L.F., Scuderi, M.M., Collettini, C., Violay, M., 2018. Do scaly clays control seismicity on faulted shale rocks? Earth Planet. Sci. Lett. 488, 59–67. https://doi.org/10.1016/j.epsl.2018.01.027.

Otsuki, K., Monzawa, N., Nagase, T., 2003. Fluidization and melting of fault gouge during seismic slip: identification in the Nojima fault zone and implications for focal earthquake mechanisms. J. Geophys. Res. 108 (No. B4). https://doi.org/10.1029/2001JB001711. 2192.

Payam, A.F., Fathipour, M., 2011. A capillary force model for interactions between two spheres. Particuology 9, 381–386. https://doi.org/10.1016/j.partic.2010.11.004.

Petit, J.P., 1987. Criteria for the sense of movement on fault surfaces in brittle rocks. J. Struct. Geol. 9, 597–608. https://doi.org/10.1016/0191-8141(87)90145-3.

Rutter, E.H., Maddock, R.H., Hall, S.H., White, S.H., 1986. Comparative microstructures of natural and experimentally produced clay-bearing fault gouges. Pure Appl. Geophys. 124, 3–30. https://doi.org/10.1007/BF00875717.

Sagy, A., Tesei, T., Collettini, C., 2017. Fault-surface geometry controlled by faulting mechanisms: experimental observations in limestone faults. Geology 45, 851–854. https://doi.org/10.1130/G39076.1.

Sibson, R.H., 1977. Fault rocks and fault mechanisms. J. Geol. Soc. 133, 191–213. https://doi.org/10.1144/gsjgs.133.3.0191.

Siman-Tov, S., Aharonov, E., Sagy, A., Emmanuel, S., 2013. Nanograins form carbonate fault mirrors. Geology 41, 703–706. https://doi.org/10.1130/G34087.1.

Smeraglia, L., Billi, A., Carminati, E., Cavallo, A., Doglioni, C., 2017a. Field- to nano-scale evidence for weakening mechanisms along the fault of the 2016 Amatrice and Norcia earthquakes, Italy. Tectonophysics 712–713, 156–169. https://doi.org/10.1016/j.tecto.2017.05.014.

Smeraglia, L., Billi, A., Carminati, E., Cavallo, A., Di Toro, G., Spagnuolo, E., Zorzi, F., 2017b. Ultra-thin clay layers facilitate seismic slip in carbonate faults. Sci. Rep. 7. https://doi.org/10.1038/s41598-017-00717-4.

Takagi, H., Kobayashi, K., 1996. Composite planar fabrics of fault gouges and mylonites—comparative petrofabrics. J. Geol. Soc. Jpn. 102, 170–179. https://doi.org/10.5575/geosoc.102.170. (in Japanese with English abstract).

Takizawa, S., 1997. Morphological observation of hydrous minerals after the freeze-drying preparation for SEM. J. Mineral. Soc. Jpn. 26, 211–214. https://doi.org/10.2465/gkk1952.26.211. (in Japanese with English abstract).

Takizawa, S., Kawata, T., Ohno, Y., 1995. A method of fixation and freeze drying of soft sediments containing water. J. Geol. Soc. Jpn. 101, 941–944. https://doi.org/10.5575/geosoc.101.941. (in Japanese).

Tanaka, H., 1992a. Cataclastic lineations. J. Struct. Geol. 14, 1239–1252. https://doi.org/10.1016/0191-8141(92)90073-6.

Tanaka, K., 1992b. Techniques for Scanning Electron Microscopy in Biology and Medicine. Kodansha Scientific, Tokyo (in Japanese).

Tisato, N., Di Toro, G., De Rossi, N., Quaresimin, M., Candela, T., 2012. Experimental investigation of flash weakening in limestone. J. Struct. Geol. 38, 183–199. https://doi.org/10.1016/j.jsg.2011.11.017.

Toda, S., Tsutsumi, H., 2013. Simultaneous reactivation of two, subparallel, inland normal faults during the Mw 6.6 11 April 2011 Iwaki earthquake triggered by the Mw 9.0 Tohoku-oki, Japan, earthquake. Bull. Seismol. Soc. Am. 103, 1584–1602. https://doi.org/10.1785/0120120281.

Tsutsumi, H., Toda, S., 2012. Surface rupture associated with the April 11, Fukushima-ken Hamadori earthquake and paleoseismic history of the causative fault. J. Geol. Soc. Jpn. 118, 559–570. https://doi.org/10.5575/geosoc.2012.0057. (in Japanese with English abstract).

Ujiie, K., Tsutsumi, A., Kameda, J., 2011. Reproduction of thermal pressurization and fluidization of clay-rich fault gouges by high-velocity friction experiments and implications for seismic slip in natural faults. Geol. Soc. Lond. Spec. Publ. 359, 267–285. https://doi.org/10.1144/SP359.15.

U.S. National Library of Medicine, 2014. Toxicology Data Network (T-BUTYL ALCOHOL). https://toxnet.nlm.nih.gov/ 15.02.19.

Yamamoto, H., Matsuyama, T., 1991. Adhesion and dispersibility of sub-micron particles. J. Soc. Powder Tech. Jpn. 28, 188–193. https://doi.org/10.4164/sptj.28.188. (in Japanese).